JOURNAL OF GEOPHYSICAL RESEARCH, VOL. 105, NO. C6, PAGES 14,045–14,060, JUNE 15, 2000

On the importance of leads in sea ice to the energy balance and ice formation in the Weddell Sea

O. Eisen[1]
Institut für Meteorologie und Klimaforschung, Universität Karlsruhe, Karlsruhe, Germany

C. Kottmeier
Institut für Meteorologie und Klimaforschung, Forschungszentrum/Universität Karlsruhe, Karlsruhe, Germany

Abstract. For a considerable coverage the energy balance of and ice formation by leads in sea ice in the Weddell Sea are evaluated on the basis of data obtained from drifting buoys for the winter periods from 1986 to 1994 and by using a kinematic-thermodynamic sea ice model. The net heat flux is defined as the sum total of radiative and turbulent fluxes. For thin ice the net turbulent flux is 3–4 times the net radiative flux. The contribution of the net heat flux through open and refrozen leads to the total net heat flux through sea ice is twice as large as the area contribution of open and refrozen leads to the total area covered with sea ice. In the eastern and central parts of the Weddell Sea, leads contribute some 30% to the total energy flux from the ocean to the atmosphere. This flux increases from 10–15 W m^{-2} in the eastern and central Weddell Sea regions to 30 W m^{-2} in the western part of the Weddell Sea, where leads contribute more than 80% of the total net energy transfer. The increase is mainly due to the colder and windier atmosphere in connection with the higher variability of the ice motion in the diurnal and semidiurnal band in the western Weddell Sea. The contribution of leads in winter ice formation exceeds 50% in the whole of the Weddell Sea. Monthly area-weighted ice growth is 10–15 cm in the east and up to 30 cm over the western continental shelf region. In the western part of the Weddell Sea, tidal and inertial motions in the diurnal and semidiurnal bands enhance lead formation, and thus contribute 7% to total net heat flux, 12% to ice formation, and 23% to the salt mass released during ice growth. The results are used to assess quantitatively the importance of leads to the interaction of the ocean, the sea ice, and the atmosphere.

1. Introduction

Roughly 10% of the ocean surface is covered by sea ice at certain times. Sea ice must be considered an important component of the global climate system. The properties of the sea ice surface effectively control the solar radiation absorbed in the ocean. Up to 90% of the downwelling solar radiation is reflected by sea ice covered with snow, and only some 10% is reflected by open water. The low thermal conductivity of snow and sea ice strongly reduces turbulent heat exchange between the ocean, cryosphere, and atmosphere in winter [*Maykut,* 1978]. The formation of sea ice also promotes ocean circulation since the density of the uppermost ocean layers is increased by cooling of the oceanic mixed layer and salt rejection into the water column during ice growth. Destabilization of the water column may initiate convection, thus contributing to the formation of bottom water. This is a major factor in ocean circulation and deep ocean ventilation [*Carmack,* 1986]. The Weddell Sea is of particular importance in the formation of bottom water as this is where the abyssal water of Antarctic origin gains its characteristics [*Fahrbach et al.,* 1994b].

Leads are openings in an otherwise closed sea ice cover that form as a result of divergent ice motion rather than local melting. Leads in sea ice allow relatively warm water to contact the air, which is up to 30 K colder in winter [*Smith et al.,* 1990]. Thus large upward turbulent fluxes of heat and water vapor are caused. As a consequence, ocean heat loss to the atmosphere reaches a maximum and high ice formation

[1]Now at Alfred-Wegener-Institut für Polar- und Meeresforschung, Bremerhaven, Germany.

Paper number 2000JC900050.
0148-0227/00/2000JC900050$09.00

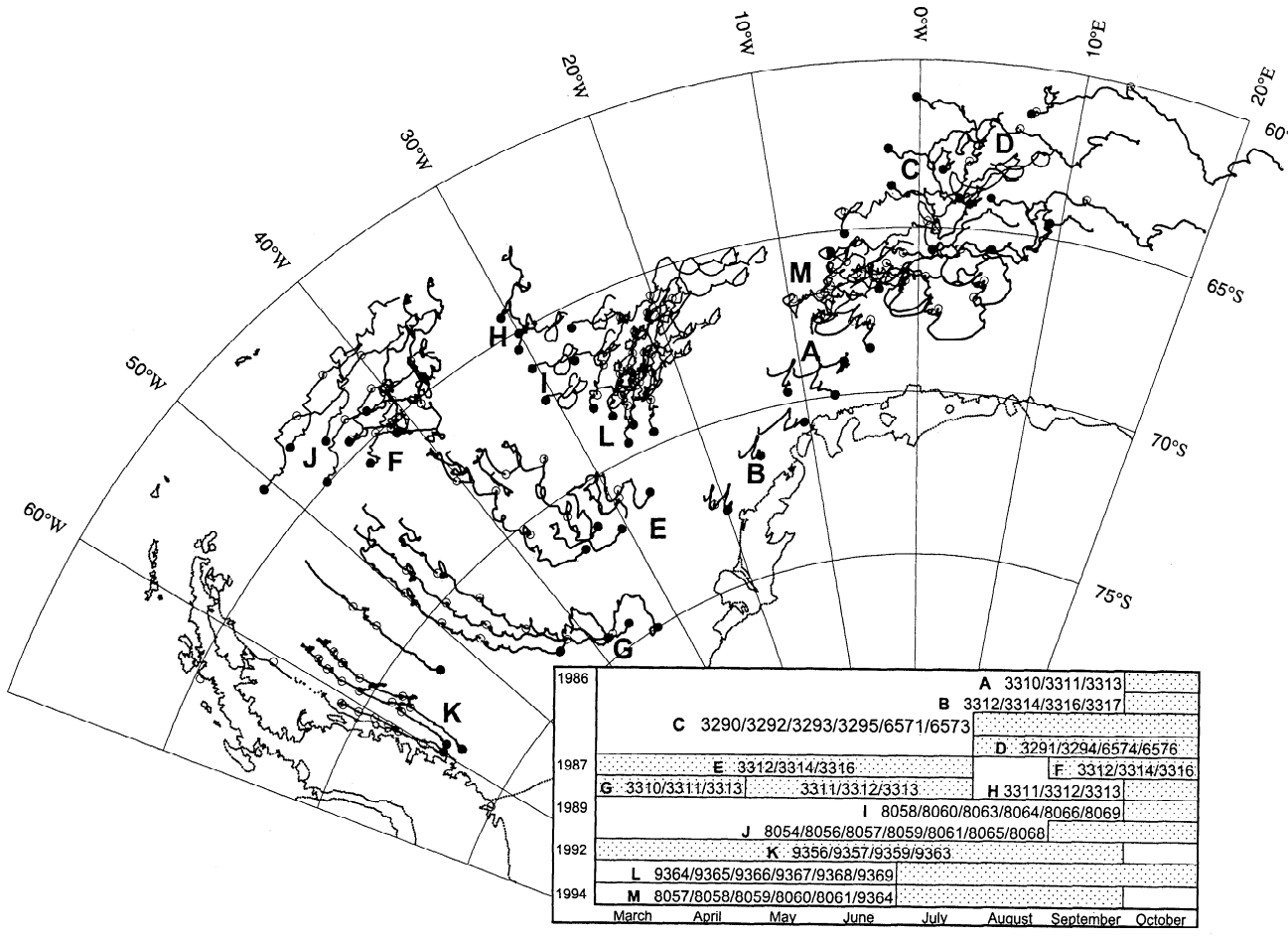

Figure 1. Map of the Weddell Sea showing the drift trajectories of the buoys used in this analysis. Several buoys were combined to form arrays, labeled A through M. The combination resulted in 14 different groups. The period of operation (years and months, shaded bars) and the buoys used for each group (indicated by the Argos Data Collection and Location System (ARGOS) identification number) are shown in the table in the lower right corner.

rates are obtained. The period of new ice formation in leads is of major importance as the rates of heat loss, ice growth, and salt rejection depend strongly on ice thickness and are up to 2 orders of magnitude higher over a refreezing lead than over perennial ice [*Maykut,* 1982]. Leads typically are kilometers to tens of kilometers long and meters to kilometers wide [*Alam and Curry,* 1997]. Experiments using a general circulation model demonstrate that the presence of leads is accompanied by large changes in the surface heat fluxes. This particularly applies to the sensible heat fluxes [*Simmonds and Budd,* 1991]. Experiments with a coupled climate-sea ice model for the Arctic reveal a zonally averaged variation in the mean annual temperature by up to 2 K for a lead percentage varying between 0 and 4.3% [*Ledley,* 1988].

In this paper a kinematic-thermodynamic sea ice model for nine classes of thin ice, based on data from drifting buoys and the analysis of the European Centre for Medium-Range Weather Forecasts (ECMWF), is used to simulate processes occurring during the freezing of leads and to calculate the resulting energy and mass fluxes. The buoys were operated in the Weddell Sea, the Atlantic sector of the Southern Ocean, between 1986 and 1994 [*Kottmeier et al.,* 1997]. The model confines calculation to leads originating from divergent ice motions. Under freezing conditions the initially open water starts to freeze because of thermodynamic growth. The terms "lead" and "thin ice" are used synonymously to characterize areas of open water and thin ice formed by dynamic processes and modified by thermodynamic growth.

The model is made up of a kinematic and a thermodynamic part. The energy balance model for thin ice, based on the model by *Maykut* [1978], represents the thermodynamic component. The air temperatures measured and air pressure gradients derived from matched buoy and ECMWF analysis data are used to calculate iteratively the surface temperature from the energy balance equation for the ice surface. All heat fluxes on the surface are estimated at a time resolution of 6 hours for all nine classes of thin ice. The energy balance at the bottom of the ice determines the thermodynamic growth rate and hence the thickness of the ice. The

kinematic part of the model determines the area of newly opened or closed leads for each time step from the differential kinematic properties of sea ice motion. The latter are recorded by buoys, which are combined in arrays of three to seven instruments [*Kottmeier and Sellmann,* 1996]. Ice thickness distribution is calculated as a function of time by linking the thermodynamic and the kinematic components. This allows the energy balance of thin ice classes, the area-weighted energy fluxes, the ice growth rate, and the salt mass released into the ocean to be determined. Comparison with the estimates for thick ice in other studies highlights the importance of leads to the energy and mass balances of the whole ice cover.

For a description of the general features the Weddell Sea is divided into three major regions. These regions show different characteristics in terms of climatology, ice thickness distribution, and oceanic regimes. The western Weddell shall be the area between 45°W and the Antarctic peninsula. This area is characterized by the continental shelf break and the permanent sea ice cover. The broad continental shelf of the southern and western Weddell Sea is said to be the source of the cold and dense Antarctic Bottom Water [*Robertson et al.,* 1995]. In this region, cold northward winds from the ice sheets dominate the mean atmospheric circulation [*Kottmeier et al.,* 1997]. The ocean current responds to the atmospheric forces by a general basin-wide cyclonic circulation. In the western Weddell Sea the northward orientation of the continental shelf break is followed by these currents in bands of higher velocities [*Kottmeier and Sellmann,* 1996]. Because of ocean circulation, the mean sea ice thickness of 1.7 m in this region is 2.5 times as thick as in the regions east of 45°W. The surface of the sea ice cover is dominated by pressure ridges. As a result, the snow layer (0.5 m) is thicker than in the central and eastern Weddell Sea (0.16 m), which is mostly covered by level ice [*Eicken et al.,* 1994]. The western Weddell Sea is mainly covered by the buoy groups K and G (Figure 1).

The Maud Rise, a subsurface seamount, and the Weddell Sea polynya are the most dominant features in the eastern Weddell Sea, the region between 10°W and 30°E. Large oceanic heat fluxes from the warm intermediate water to the surface may reduce ice thicknesses, thus causing more heat to be transferred from the ocean to the atmosphere [*McPhee et al.,* 1996]. The temperature distribution exhibits a south-north gradient, westerly winds prevail north of 65°S, and coastal easterly winds prevail south of 65°S, both very variable because of low-pressure systems [*Kottmeier et al.,* 1997].

The region between 45° and 10°W is referred to as the central Weddell Sea. In the northern part the temperature and wind distributions are similar to those in the eastern Weddell Sea. In the southern part, however, katabatic winds from the Antarctic ice sheet result in southeasterly winds along the coast [*Kottmeier et al.,* 1997]. A prominent feature of ocean circulation is the strong coastal current along the southeastern coast and the front of the ice shelves in the south [*Fahrbach et al.,* 1994a].

Analysis of the regional differences in the physical environments of the three regions reveals spatial differences of the energy and mass balances for the Weddell Sea. The influence of tides on the processes in leads becomes obvious.

2. Sea Ice Model

The heat losses through leads in the sea ice zone far from the coast are calculated with an energy balance and thickness model for thin ice. Model calculations are restricted to thin and young ice with a maximum thickness of 90 cm. Usually, the thickest ice class of 60–90 cm is not occupied. Ice thicker than 90 cm, which is produced by thermodynamic growth or dynamic processes, such as rafting and ridging, is not considered explicitly. The major data of the model are the air temperature, ice drift divergence, and geostrophic wind speed as determined by the buoy measurements, which covered regions of ~10,000–50,000 km^2 (Figure 1) [*Kottmeier and Sellmann,* 1996]. The database is described in detail below.

2.1. Kinematics

In the kinematic part of the model, sea ice is two-dimensional. The mean and differential motions are represented by the buoy drift. Thus the horizontal components only are used for all tensor quantities.

The kinematic properties are calculated by fitting the buoy drift vector $\mathbf{d} = (d_x, d_y)$ to a linear combination of the geographical position $\mathbf{r} = (x, y)$ [*Kottmeier and Sellmann,* 1996]. This has the form

$$\mathbf{d}(x, y) = \mathbf{U}\,\mathbf{r}(x, y) + \mathbf{v}. \tag{1}$$

Because of their smoothing effect on measurement errors, first-order polynomials are more suited for fitting ice drift components than second-order polynomials [*Kottmeier and Sellmann,* 1996]. The components of the matrix $\mathbf{U} = u_{ij}$ $(i, j = x, y)$ and the vector $\mathbf{v}$ are determined for each time step t of buoy data by least squares fitting. Regression of the buoy data by (1) furnishes a time series u_{ij} with a time resolution of $\Delta t = 6$ hours. Using the horizontal gradient operator $\nabla_h = (\partial/\partial x, \partial/\partial y)$, the drift divergence

$$\nabla_h \cdot \mathbf{d} = \nabla_h \cdot (\mathbf{U}\,\mathbf{r} + \mathbf{v}) = u_{xx} + u_{yy} \tag{2}$$

is used to calculate the area $A_{t+\Delta t}$ of the buoy field after a time step Δt given by

$$\begin{aligned} A_{t+\Delta t} &= A_t + \Delta A_t = A_t + A_t \nabla_h \cdot \mathbf{d}_t\, \Delta t \\ &= A_t\,[1 + (u_{xx} + u_{yy})\,\Delta t]\,. \end{aligned} \tag{3}$$

A_t is the area of the buoy field at the time t. The ice thickness distribution within a buoy field is derived on the basis of the assumption that fluctuations in the divergence of the ice drift are mainly the opening and

closing of leads between the thicker floes. The percentage of leads can thus be inferred from the change in the area ΔA_t enclosed by the polygon drawn through the outermost buoy positions. Freezing and the change in ice thickness of leads are calculated for all ice classes on the basis of a balance of all heat fluxes involved. Hence the lead percentage solely depends on the drift divergence obtained from buoys. The buoys are assumed to be properly spaced and arranged so as to represent the mean divergence of ice motion on the scale of 10^4 km^2. Data from analyses where buoys are located too close to each other and where their arrangement became too linear to derive both spatial derivatives were excluded.

Thorndike [1986] used a simple model to examine the possibility of predicting the opening and closing of the ice pack by means of the invariants of the matrix u_{ij}. A large number of Gaussian-distributed velocity fields only yielded a weak relation between the simulated deformation of the pack and the invariants. During the Winter Weddell Sea Project, *Kottmeier et al.* [1992] calculated the spatial correlation lengths of the buoy drift speeds and components. The longitudinal correlation lengths of the drift speeds varied between 490 and 680 km; the lateral ones varied between 270 and 540 km. *Vihma et al.* [1996] determined correlation lengths of 700 km for the longitudinal and 550 km for the lateral drift speeds in the central and western Weddell Sea. As a result of the large correlation lengths, the spatial ice drift gradients seem to have been resolved adequately by first-order polynomials. In addition, fluctuations of the ice drift divergence as derived from buoy motions are considered to be measures of changes in leads.

2.2. Energy Balance

The thermodynamic part follows the approach by *Maykut* [1978]. The surface energy balance

$$F_r - F_R - I_0 + F_L - F_E + F_s + F_e + F_c = \begin{cases} 0 & T_0 < T_f \\ F_m & T_0 \geq T_f \end{cases} \quad (4)$$

combines the incoming shortwave radiation F_r, the reflected solar radiation $F_R = \alpha F_r$, the radiative flux I_0 passing through the surface into the interior of the ice, the incoming and outgoing longwave radiation, F_L and F_E, respectively, the sensible and latent heat fluxes, F_s and F_e, and the conductive heat flux F_c through the ice. When the surface temperature T_0 exceeds the melting temperature T_f, F_m is introduced. It denotes that part of energy on the surface of the ice that is used to melt ice and keep T_0 at the melting point. Only the F_r and F_L components of the surface energy balance of sea ice are independent of ice thickness. All other fluxes depend on the thickness of the ice either explicitly or via the surface temperature.

At the bottom the ice grows thermodynamically according to

$$-\rho_i L_f \frac{\partial h}{\partial t} = F_o - F_c, \quad (5)$$

where the oceanic heat flux is F_o, $L_f = 334.8$ kJ kg^{-1} is the latent heat of fusion, and $\rho_i = 910$ kg m^{-3} is the ice density [*Maykut,* 1982]. For the sake of brevity, only those quantities will be described in detail that differ from the parameterizations performed by *Maykut* [1978].

Incident solar radiation on the surface is calculated as [*Maykut,* 1986]

$$F_r = \kappa Q_0. \quad (6)$$

Here the cloud correction term according to *Laevastu* [1960],

$$\kappa = 1 - 0.6c^3, \quad (7)$$

takes into account the cloud cover c, which is taken to be constant as $c = 0.6$. Solar radiation Q_0 is taken from *Zillmann* [1972]. It is commonly used for polar regions [*Parkinson and Washington,* 1979; *Maykut,* 1986]. Here the albedo is calculated from a logarithmic function $\alpha(h) = b_1 \ln(h/b_2)$ fitted to the values provided by *Maykut* [1978]. The constants result as $b_1 = 6.78 \times 10^{-2}$ and $b_2 = 9 \times 10^{-4}$ m. Shortwave radiation penetrating the ice surface has the form of

$$I_0 = i_0 (1 - \alpha) F_r, \quad (8)$$

where the parameter $i_0 = 0.18(1 - c) + 0.35c$ is taken from *Grenfell and Maykut* [1977]. The Stefan-Boltzmann law

$$F_{E/L} = \epsilon_{0/a} \sigma T_{0/a}^4 \quad (9)$$

is used for longwave radiation, with the surface temperature T_0 and air temperature T_a for the upwelling and downwelling fluxes, F_E and F_L, respectively. Longwave emissivity of the surface ϵ_0 is taken to be 0.97. For atmospheric emissivity ϵ_a we use the parameterization of

$$\epsilon_a = 0.765 + 0.22c^3 \quad (10)$$

derived by *König-Langlo and Augstein* [1994]. For the cloud cover a constant value of $c = 0.6$ is applied.

The turbulent fluxes are calculated from aerodynamic bulk formulae according to

$$F_s = \rho c_p C_s V_{10} (T_a - T_0) \quad (11)$$

$$F_e = \rho L_v C_e V_{10} (q_a - q_0), \quad (12)$$

where ρ is the air density, c_p is the specific heat, V_{10} is the wind speed at a height of 10 m, and q is the specific humidity. To take wind and stability effects into account, the transfer coefficients of sensible and latent heat, C_s and C_e, are calculated from the scheme derived by *Kondo* [1975]. As no wind measurements are available, the wind speed is calculated from the geostrophic wind using modified transfer cofficients C_s and C_e. According to the analysis performed by *Kottmeier et al.* [1992], using geostrophic wind speeds instead of wind speeds measured at the buoy locations is justified. To express q and thus F_e as a function of T_0 and T_a, the

parameterization described in detail by *Maykut* [1978] will be employed.

Conductive heat flux through a thin slab of ice can be calculated as the product of the thermal conductivity of sea ice and the linear temperature gradient [*Maykut*, 1978]:

$$F_c = \left(k_0 + \frac{\beta S_i}{T_i - T_{f,0}}\right)\left(\frac{T_b - T_0}{h}\right). \qquad (13)$$

Here $k_0 = 2.03$ W m^{-1} K^{-1} is the conductivity of pure ice. $\beta = 0.117$ W m^2 kg^{-1} (practical salinity units (psu))$^{-1}$ is a constant. $T_{f,0} = 273.15$ K is the melting temperature of pure ice. Thermal conductivity of sea ice thus depends on the salinity S_i and the temperature T_i of the ice. The second term denotes the linear temperature gradient in the slab, where $T_b = -1.88$°C is the temperature at the bottom of the ice for a water salinity of 35 psu. Thermal conductivity is calculated using the mean ice temperature $T_i = (T_0 + T_b)/2$. Doing this, unrealistic thermal conductivity values for surface temperatures close to the melting point can be avoided in the salinity range studied

The salinity of thin sea ice strongly depends on ice thickness. For ice thinner than 10 cm, observation data are sparse. To express salinity as a continuous function of thickness between 3 and 90 cm, a power series of the form

$$S_i(h) = a_{-1}h^{-1} + a_0 + a_1 h \qquad (14)$$

is fitted to the values given by *Maykut* [1978], *Wakatsuchi* [1983], and *Melnikov* [1995] (Figure 2). With

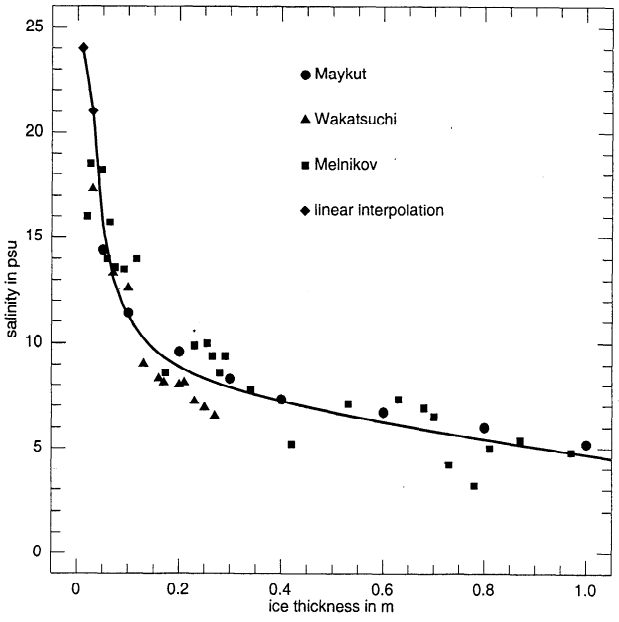

Figure 2. Salinity of sea ice as a function of ice thickness. The data measured by *Maykut* [1978], *Wakatsuchi* [1983], and *Melnikov* [1995] are fitted with the power series (14) for a thickness range of 3–90 cm. The values between 1 and 3 cm are linearly interpolated.

h expressed in m and S_i expressed in psu, the constants are $a_{-1} = 0.4089$ psu m, $a_0 = 7.477$ psu, and $a_1 = -3.196$ psu m^{-1}. Under calm wind conditions, thin ice is formed homogeneously. Under windy conditions, turbulence on the water surface causes frazil ice to form and consolidate to grease ice consisting of ~30% ice and 70% seawater [*Bauer and Martin*, 1983]. At a salinity of seawater of 35 psu, grease ice is supposed to have a salinity of ~24 psu. Since no measurements are available for ice of 0–3 cm in thickness, this salinity value is assigned to the thinnest ice investigated ($h = 1$ cm). Values for ice in the range of 1–3 cm are linearly interpolated from this value to the power series value for a thickness of 3 cm.

The parameterization described above allows all energy fluxes on the ice surface to be written as a function of the surface temperature or to be known independently. T_0 can be obtained from (4) by Newton's iterative method as described by *Maykut* [1978]. A study for comparison of this scheme with satellite surface thermometry has been carried out and will be published elsewhere [*Veihelmann et al.*, 2000]. For open water the surface energy balance (4) slightly differs from that of thin ice. The flux I_0 penetrating the ice surface is replaced by the flux I_w absorbed by the upper oceanic layer. I_w is a function of cloudiness, the albedo of water set to 0.1, and the parameter $i_w(H)$ determining the net shortwave radiation transmitted by a water layer of the thickness H [*Maykut and Perovich*, 1987]. Oceanic heat flux F_o directly contributes to the surface energy balance. There is no conductive heat flux F_c. Under the assumption of the water permanently equalling the freezing point, $T_0 = T_b$, all fluxes depending on T_0 and the thermodynamic growth rate can be calculated. If there is a net heat gain on the surface, the additional energy does not cause any significant local warming as it is assumed to be homogeneously distributed in the lead and underneath the neighboring pack ice because of the relative motion of floes and water [*Maykut and Perovich*, 1987].

2.3. Coupling of the Kinematic and the Thermodynamic Schemes

The surface energy balance (4) is solved at each time step for nine classes of thin ice and one class of open water. The thickness classification is shown in Table 1. The area covered by sea ice of a specific thickness class changes because of dynamic and thermodynamic effects. The area of class k ice is transferred to class $k+1$ when its thickness reaches the upper thickness limit. It increases when thinner ice of class $k-1$ reaches the lower thickness limit of class k and vice versa for melting. With a positive divergence at a certain time, $A_{t+\Delta t} - A_t$ is added to the area of open water (class 0) to account for the formation of new leads. When the ice motion is convergent, the open water and the thinnest ice are assumed to be removed first. The next classes of thicker

Table 1. Classification of Ice Thicknesses

Coverage	Ice Class k	Ice Thickness, cm
Open water	0	0-1
	1	1-3
	2	3-5
	3	5-7
	4	7-10
Thin ice	5	10-15
	6	15-20
	7	20-40
	8	40-60
	9	60-90
Thick ice	10	> 90

ice may also be affected during periods of strong convergence. The ice removed from the lead ice classes during convergence is assumed to be attached to ice floes of the thickest ice class (class 10). As the effects of open and refrozen leads is of particular interest, the contribution of the thickest ice class to the energy and mass balances of the area covered by the buoy array is evaluated using empirical data (see section 2.4) rather than model calculations. Hence the ice mass is conserved in the model by means of class 10, which is a reservoir filled by transfer of ice from other classes during convergent sea ice motion and ridge formation.

The minimum area during the period of operation is considered to represent 100% ice concentration, that is, no ice with an ice thickness of 0–90 cm is present. Now the area of the buoy array is assigned to the thickest ice class. At all other times a certain amount of thin ice with a thickness between 0 and 90 cm is present. Since the initial area distribution within all classes is not known, it is assumed to be identical to the average distribution and corrected iteratively using several model runs. The effects of rafting, ridging, and the snow cover, though desirable, have not been included in the model. We argue that this does not make our results unrealistic. The problem with rafting is that no solid parameterizations seem to be available. In addition, the model cannot predict the size distribution of leads within a certain area. However, this parameter is necessary to predict the rafting of the thin ice classes more accurately than the assumption described above.

To determine the snow cover, the frequency distribution and the amount of snowfall are required. Despite the low conductivity of snow this effect will not play a dominating role. Snow rapidly melts in open leads and leads covered by thin ice with a large liquid water content, especially when rafting occurs. With the ice cover getting thicker the presence of thin snow on top loses influence since its heat conduction generally is smaller than that through thin ice.

2.4. Database

The buoy fields of each experiment are divided into several groups representing different seasons, regions, and ice conditions. This results in 14 buoy groups making up the general database (Figure 1). The geostrophic wind speed and drift velocity are calculated according to *Kottmeier and Sellmann* [1996]. To account for the errors resulting from uncertainties of the buoy position, the standard deviation of white noise is removed from the drift divergences by using the errors given by *Kottmeier and Sellmann* [1996]. The air temperature series are corrected by replacing unrealistic values by a value that is linearly interpolated from the neighboring values of the time series.

The oceanic heat fluxes used to calculate the mass balance at the bottom of the ice are taken from different measurements in the Weddell Sea. Because of the lack of individual measurements of the ocean heat flux for the different buoy arrays, the value of 19 W m^{-2} estimated by *Martinson* [1994] is used for all buoy arrays except for the westernmost and easternmost ones, i.e., the arrays related to Ice Station Weddell (ISW) and the Antarctic Zone Flux Experiment (ANZFLUX). In the ANZFLUX project the heat flux was measured by turbulence probes and estimated by thermistor strings for the subsequent period [*McPhee et al.*, 1999]. This resulted in a time series of ocean heat flux that was used to set the buoys of the ANZFLUX array. The mean value of ocean heat flux obtained during the measurements from July 30 to October 14, 1994, was 27.4 W m^{-2}. The mean values of the oceanic heat flux measured over the continental shelf in the western Weddell Sea by ISW in 1992 are also taken into account. The ocean heat flux was estimated by several authors using different means. *Lytle and Ackley* [1996] determined the energy flux from the temporal development of the snow and ice coverage as well as from measurements of the temperature profile of the ocean mixing layer. The mean ocean heat flux was 7 ± 2 W m^{-2} for the period from the end of February to the beginning of June 1992. We believe that their values are more suitable for the application of the model as they are derived directly from observations of ice thickness and therefore also include the influence of shortwave radiation absorbed in leads. This is not the case for heat fluxes derived from conductivity-temperature-depth profiles (CTDs) at depths of 100-350 m [*Robertson et al.*, 1995] and internal gravity waves and tides [*Levine et al.*, 1997], which result in a mean ocean heat flux of 1.7 and 1.0 W m^{-2}, respectively. Conductive heat fluxes through thick ice are included by using empirical data based on local short-term studies by *McPhee et al.* [1999] and *Lytle and Ackley* [1996] as well as large-scale estimates by *Fahrbach et al.* [1994a].

3. Accuracy and Sensitivities

The thickness distribution and energy balance of ice provide the basis for calculations of the transfer of energy from the ocean to the atmosphere. To estimate the accuracy of the model, two comparisons, i.e., in situ ice thicknesses and ice concentrations derived from Special Sensor Microwave Imager (SSM/I) data, are performed

using independent methods. The influences of parameterizations and errors on the decisive meteorological quantities are investigated in several sensitivity studies.

3.1. Ice Growth Rates

Ice growth rates in newly formed leads were observed in several experiments [*Melnikov,* 1995] performed at ISW in 1992. Meteorological data from the ISW experiment and the atmospheric pressure field as defined by buoy and ISW air pressure data allow the freezing of a lead to be simulated by the model. The first experiment comprised observations of ice growth in test holes of 1 m^2 area drilled into the refrozen lead. It started at 0000 UTC on May 20. The mean ice growth rates were 0.30 cm h^{-1} during the first 24 hours, resulting in an ice thickness of 9.13 cm. They decreased to 0.14 cm h^{-1} over the next 7.5 days [*Melnikov,* 1995]. For the same period our model calculates ice growth rates of 0.31 and 0.17 cm h^{-1}, respectively. In a second experiment, ice cores were taken every 7–10 days from a second lead covered by young sea ice. Between March 18 and May 28, ice thickness increased from 42 to 78 cm [*Melnikov,* 1995], which corresponds to a mean growth rate of 0.32 mm h^{-1}. The model yields a mean growth rate of 0.46 mm h^{-1}. Good agreement is found between in situ measurements and modeling, especially for thin ice. Systematic overestimation of the growth rates by 18 and 30% for ice thicker than 10 cm in the first and second experiments is most likely due to the neglection of the insulating snow cover. The use of a constant oceanic heat flux instead of a time series as well as the different conditions under which the measurements and the simulations are performed, i.e., the air temperature measured at the main camp and not at the lead site, might provide some explanation.

3.2. Ice Concentrations From the Model and SSM/I Data

The coupled thermodynamic and kinematic model is tested best by investigating the ice thickness distribution. The thickness distribution of sea ice can be measured by moored upward looking sonars. However, no method is available for arbitrary regions and periods [*Strass and Fahrbach,* 1998]. Currently, the most suitable data for comparison are ice concentrations derived from passive microwave radiometers. For the time before 1992 the ice concentrations calculated from the DMSP SSM/I using the NASA Team algorithm [*Cavalieri et al.,* 1984] were used. For the time since 1992 the data set published by the Project for Estimation of Long-Term Variability in Ice Concentration (PELICON) [*Heygster et al.,* 1996] is applied. We decided to use the NASA Team algorithm as it provides more consistent ice concentrations over different regions and years than, for example, the bootstrap algorithm [*Heygster et al.,* 1996].

The ice concentration of a region is defined as the ratio of the ice-covered area to the total area. In satellite remote sensing the antenna footprint size determines the extension of the region to which an ice concentration is assigned. Analysis of the DMSP SSM/I data with the NASA Team algorithm leads to a spatial resolution of ~30 × 30 km^2 [*Heygster et al.,* 1996]. Calculating the ice concentration from buoy data is only possible for the complete area of the buoy array. Usually, it is of the order of 10^4 km^2.

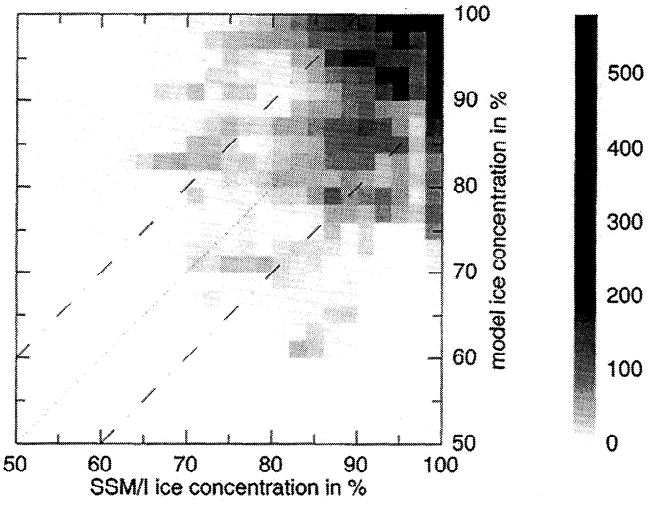

Figure 3. Density distribution of the model-based and SSM/I ice concentration data pairs. The gray scale defines the number of data pairs within a square of $2\times2\%^2$. The mean difference between model-based and SSM/I concentrations is −0.01%, with a standard deviation of 10.4%.

According to the sensitivity study performed by *Comiso et al.* [1992] the presence of new ice causes the ice concentration to be underestimated by SSM/I algorithms because of the variable emissivity of new ice. These ice concentrations do not represent the absolute amount of open water but include newly formed ice as part of the open water. To take this effect into account when comparing buoy and SSM/I-derived ice concentrations, the model calculates several ice concentrations. Here all ice below a certain thickness is assigned to the area of open water.

For investigating the relation between the model-based and the corresponding NASA Team ice concentrations both values are plotted versus each other using a density distribution (Figure 3). For each time of the data series the model and NASA Team concentrations are combined in pairs, thus yielding 11,788 data pairs for the period between March and October of the years 1987-1994. Because of the restriction to winter months, most pairs are located at the high ice concentration end of the scale. Both the model-based and the SSM/I concentrations range between ~70 and 100%, with a maximum occurring at 98–100%. This becomes even more obvious when counting the number of data pairs within a $2 \times 2\%^2$ period and showing a gray scale increasing with the number of pairs for each square instead of just plotting the data pairs (Figure 3). The range of val-

ues covered by both data sets is thus too small for a reasonable statement to be made with regard to the correlation coefficient of both data sets. Therefore the mean difference is used to evaluate the relation between both data sets.

Both methods require the thresholds to be defined in order to distinguish the fractions of "leads, new ice, thin ice" and "thick ice". A definition in terms of brightness temperatures is needed for the SSM/I radiometer, and for the model case in terms of ice thickness classes. The mean difference between model-based and NASA Team ice concentrations is smallest if the area of ice with <36 cm in thickness is considered a lead fraction when calculating the model ice concentration. In this case the standard deviation equals 10.4%. Therefore a threshold value of 36 cm is adopted for calculating the ice model concentrations.

According to *Steffen et al.* [1992] the SSM/I ice concentrations evaluated with the NASA Team algorithm underestimate the ice concentration by 5–15% at high concentrations. If an error of 10% is assumed for the SSM/I data that adds up to the errors resulting from the different spatial resolutions of the methods, a significant proportion of the differences can be explained. The error estimate of 10% from Arctic comparisons even is conservative for the Weddell Sea since ice concentrations obtained from a Landsat scene differed from the team algorithm by 35% [*Steffen and Schweiger,* 1991]. The model ice thickness distribution may therefore be concluded to represent the true distribution with an error of 10–15%.

3.3. Sensitivity Studies

The sensitivity of output quantities to modified parameterizations and systematically altered decisive data is investigated as well. While changing the value or physical parameterization for one quantity, all other parameters and time series remain constant. Any changes in the output quantities are thus, in first order, related to the change of a single decisive input parameter.

For observing the reaction of the model to a change in the input data set, five quantities are used: the net heat flux, the sum of the turbulent heat fluxes, the radiation balance, the ice growth rate, and the surface temperature. All these quantities for the thin ice classes are weighted by area and converted to the total area of a buoy array. As mainly time-averaged quantities will be discussed in sections 4 and 5 the output values are averaged over the buoy array's lifetime instead of investigating changes in the time series of the output quantities. In the following paragraph the influence of the most important parameters as obtained from a number of sensitivity experiments will be highlighted using the ANZFLUX buoy array as an example. Discussion will be restricted to the most important output parameters, i.e., the net heat flux and the ice growth rate.

The albedo parameterization is set constant in the range from 0.2 to 0.8. For the ANZFLUX data this results in a change of <4% of the net heat flux and ice growth rate. Considering the albedo variation range, these changes are comparably small. Using values between 0.3 and 0.9 for the cloud cover, the variation of the output parameters is comparable to that resulting from the albedo variation. Use of constant values in the range of 1.0×10^{-3} to 3.0×10^{-3} instead of the wind- and stability-dependent parameterizations for both turbulent transfer coefficients leads to a variation of the growth rate of 19% and a variation of the net heat flux of 7%.

The sensitivity of the model to the measured air temperature is tested by systematically increasing and decreasing the time series for T_a by 1 K, respectively. A temperature offset of ±1 K results in a change of the net heat flux of $\sim\mp 25\%$. The ice growth rate is even more affected. It decreases by 45% for a 1 K increase and increases by 35% for a 1 K decrease of the air temperature time series.

A systematic increase and decrease of the wind speed time series is found to be less pronounced in the output data. Altering the wind speed by ±30% results in a change of the net heat flux of ±2% and of the ice growth rate of <±7%.

The influence of the ocean heat flux is investigated by comparing the results of the standard runs with a run in which the time series of the ocean heat flux was set to zero. The effect of the ocean heat flux on the radiative and turbulent heat balance due to a changed ice thickness distribution can be neglected. The net heat flux is reduced by ~10% when neglecting the ocean heat flux. Ice production remains almost unchanged for ice between 0 and 20 cm in thickness. However, it increases by ~25% if all classes of thin ice are considered. A detailed dicussion of the influence of the ocean heat flux on the ice cover as well as of the heat exchange will be published elsewhere.

To sum up, the average heat fluxes, ice growth rates, and surface temperatures are more sensitive to variations of wind data and measured air temperatures than to reasonable changes in the physical parameterizations of the model. The physics may therefore be concluded to be presented with sufficient accuracy by the model. However, care must be taken when selecting the major input data. At a given error of ~1 K for the measured air temperature the net heat flux from the ocean to the atmosphere has an accuracy of 3.5 W m^{-2}. The monthly ice growth rate is determined with an accuracy of 4.5 cm. At a wind inaccuracy of 15% the resultant error is 0.23 W m^{-2} for the net heat flux and 0.75 cm for the monthly growth rate.

4. Results

The buoy data can be used to investigate in detail the physical interactions in a certain area, i.e., at the location of a buoy array. They also allow the comparison of the results for different regions on a longer timescale. In section 4.1 some results will be presented with respect

to the influence of leads on the ice thickness distribution, the composition of the surface energy balance as a function of ice thickness, and on other quantities. A buoy array in the western Weddell Sea is chosen for this purpose. In section 4.2 the data from all 14 groups, collected between 1986 and 1994, are used to evaluate the regional differences and characteristics of heat flux and ice production in the Weddell Sea. Thus the regional distributions of the net heat flux, ice production, and salt release shall be evaluated.

4.1. Importance of Leads to the Heat Transfer and Mass Balance

By way of example the results furnished by the model are presented for one buoy of the buoy array located in the western Weddell Sea in 1992. A continuous data set from March 1 to September 5, 1992, is available. The changes in thickness and area of two ice classes in response to the meteorological and kinematic data of sea ice between April 16 and May 4, 1992 (Figure 4), demonstrate the interacting influence of air temperature and divergence on the ice thickness distribution.

For this period the air temperature reaches a maximum at t_1 (April 19, day of year 110). The area of the buoy array reaches its largest extent just before t_2 (April 22, day of year 113) and experiences a minimum at time t_4. The high air temperature at time t_1 causes the ice growth rate to stagnate as is shown for the development of ice thickness in class 7 (Figure 4). At the same time, no ice of class 6 is present. Before and after this time the ice growth rate becomes more pronounced because of lower temperatures. At time t_2 the ice thickness in class 7 reaches its upper limit. Its area is transferred to the next thicker ice class, and the ice thickness is reset to the lower limit value. From t_2 to t_3, divergence mostly is negative. As a consequence, the total area of the buoy array decreases. To compensate this reduction, the area of the thinnest ice classes is reduced. Ice thickness of class 6 reaches its upper limit at t_3. The area transferred from class 6 to class 7 is also affected by the area decrease. It is used to offset the reduction as there is no longer any area found in the classes below 15 cm thickness. From t_4 to t_5 divergence is entirely positive. Therefore open water exists that starts to freeze over. Its area is transferred to thicker classes (not shown). At time t_5, area is transferred from class 5 (not shown) to class 6. As the ice growth rate is high because of low temperatures, the upper thickness limit of class 6 is reached within 1 day, and the area is transferred to class 7.

Conductive heat flux, which is identical to the net heat flux to the atmosphere for thin ice [*Maykut*, 1978], is higher in open water and thin ice by ~1 order of magnitude than in thick ice (Figure 5). For open water the incoming longwave and shortwave radiation, 182 and 26 W m^{-2}, make up some two thirds of the outgoing longwave radiation of -298 W m^{-2} (Table 2). Turbulent fluxes of -474 W m^{-2} are the main contributors to the net heat transfer of -567 W m^{-2} to the atmosphere. For ice thicknesses between 60 and 90 cm the incoming radiative fluxes almost equal the outgoing longwave radiation of -223 W m^{-2}. Here the turbulent fluxes provide nearly half of the net heat flux of -55 W m^{-2}, but the radiative balance also has to be accounted for under winter conditions.

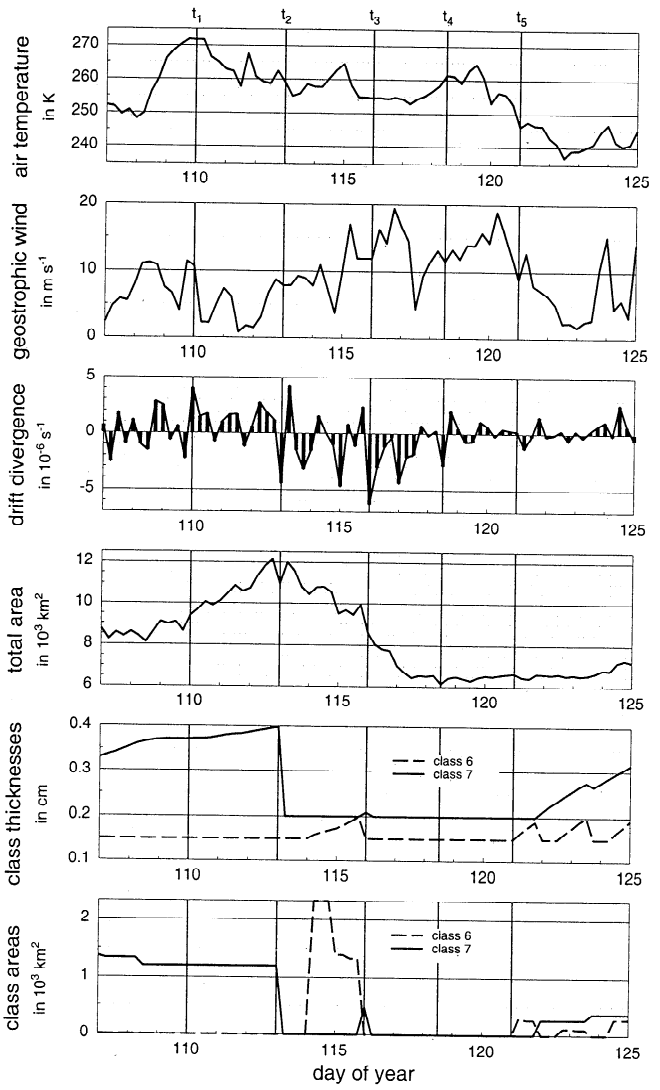

Figure 4. Example of the response of ice thickness and the area of ice classes 6 and 7 to forcing data for the period between April 16 and May 4, 1992 (days of year 107-125). The forcing data are the air temperature T_a, geostrophic wind speed V_g, and drift divergence $\nabla \cdot \mathbf{d}$. The times $t_1 - t_5$ mark changes in the area and thickness distributions of ice classes, as described in the text.

Consequently, the relative contributions of open and refrozen leads to the net heat transfer are larger than their percentage areas of the total ice cover (Figure 6). Accordingly, ice production and, in particular, salt release mainly take place in leads. The net flux of heat into the atmosphere, relative to the area and summed up over all thin ice classes and thick ice, is 40.4 W m^{-2}. It causes an equivalent ice production of the total ice cover, defined as the area-related production of all classes

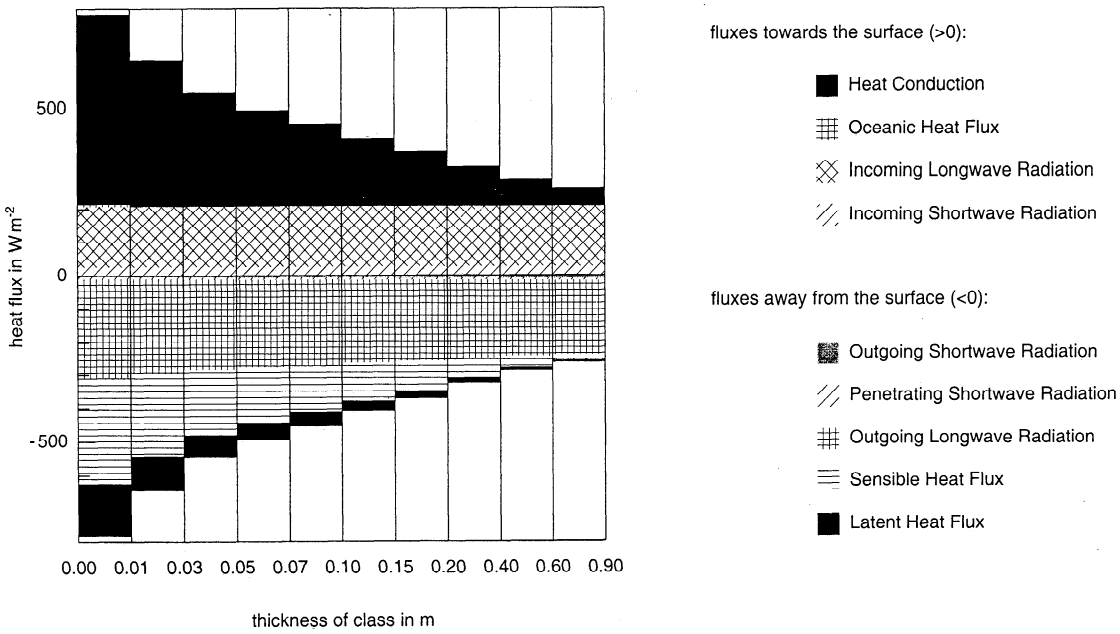

Figure 5. Components of the energy balance for thin ice classes, averaged between March 1 and September 5. For the quantity of the fluxes, see also Table 2.

of thin and thick ice, of 36.2 cm $(\text{month})^{-1}$. Because of the imbalance of oceanic and conductive heat fluxes, ice production under thick ice makes up 2.9 cm of total ice production. Only ~8.0% of the ice mass is formed under thick ice. The major proportion is formed under ice of <30 cm in thickness. More than 90% of the mean monthly salt flux of 1.42 kg m^{-2} is released from ice of <25 cm in thickness.

4.2. Regional Comparison

On the basis of the data from all 14 buoy groups a regional distribution of the most important physical properties of the ocean-ice-air interaction is obtained. When calculating the gridded regional distribution, the scheme described in detail by *Kottmeier and Sellmann* [1996] is used. It is based on 30 days' mean values of the considered parameter and the buoy position. A weighted mean value within a radius of acceptance is assigned to each grid point. To avoid major uncertainties due to unknown properties of the ice cover at the beginning and end of the melting season, the analysis is restricted to the months of March through October. Interannual differences in the length of the ice season of the Weddell Sea, as obtained from SSM/I data [*Parkinson,* 1998], are not considered. To distinguish between the influences of spatial and seasonal changes, a cosine

Table 2. Energy Balance Components at the Ice Surface for Thin Ice Classes

Flux	Ice Class k									
	0	1	2	3	4	5	6	7	8	9
F_c	567.2	438.1	339.9	287.6	245.0	200.7	161.6	117.1	78.2	54.8
F_o	7.0	...	...	...	...	...	...	...	...	...
F_L	181.7	181.7	181.7	181.7	181.7	181.7	181.7	181.7	181.7	181.7
F_r	26.3	26.3	26.3	26.3	26.3	26.3	26.3	26.3	26.3	26.3
F_R	-2.6	-4.5	-6.3	-7.2	-7.9	-8.6	-9.2	-10.1	-11.1	-11.9
I_0	-7.3	-6.1	-5.6	-5.4	-5.2	-5.0	-4.8	-4.6	-4.3	-4.1
F_E	-298.2	-282.9	-270.4	-263.1	-256.9	-249.9	-243.5	-235.5	-228.1	-223.4
F_s	-317.0	-250.9	-197.2	-166.7	-140.8	-113.4	-88.4	-59.5	-33.5	-17.7
F_e	-157.1	-101.7	-68.4	-53.2	-42.2	-31.9	-23.7	-15.5	-9.2	-5.8

The fluxes are the values of each ice class averaged from March 1 to September 5. All fluxes are given in W m^{-2}. The ocean heat flux F_o contributes only to the surface heat balance for open water (class 0). The variables are: F_c: heat conduction, F_o: oceanic heat flux, F_L: incoming longwave radiation, F_r: incoming shortwave radiation, F_R: outgoing shortwave radiation, I_0: penetrating shortwave radiation, F_E: outgoing longwave radiation, F_s: sensible heat flux, F_e: latent heat flux.

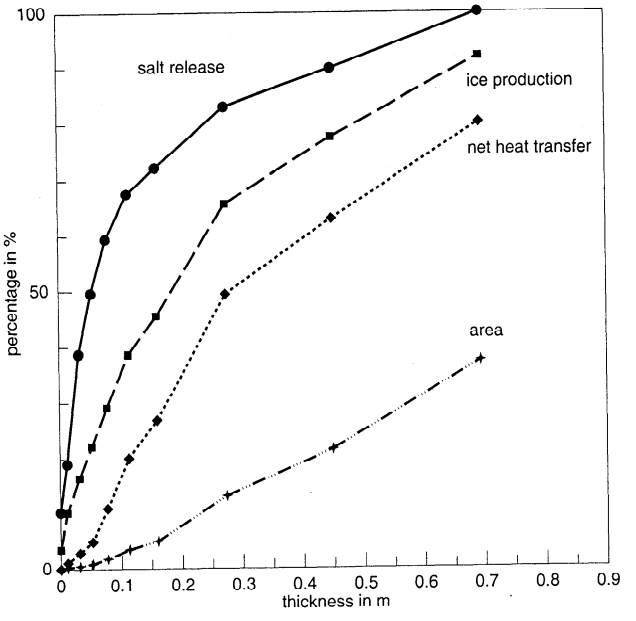

Figure 6. Time-averaged percentage of area, net heat flux, ice production, and salt release for the period from March 1 to September 5 as a function of ice thickness. The values are cumulated over the ice classes. The total net heat flux summed up over all classes of thin ice and thick ice is 40.4 W m^{-2}, the corresponding total monthly ice production 36.2 cm, and the total monthly salt release 1.42 kg m^{-2}.

function is fitted to the deviations of the gridded field as a function of the respective day. The relative variance explained by the cosine function is a measure of seasonal influences that are not explained by the gridded composite field [*Kottmeier and Sellmann,* 1996].

Energy transfer into the atmosphere through the area of open water and thin ice is a measure of ice growth productivity of the leads. It is determined primarily by the atmospheric and oceanic activities considered for the energy balance. The ratio of thin ice to thick ice areas is additionally taken into account by the relative area fractions of the two categories. The resultant quantity describes the contribution made by leads to the total energy transfer as compared to the heat flux over thick ice.

In the central and eastern Weddell Sea the distribution of the heat flux through open water and thin ice, relative to the area, is relatively homogeneous. West of 45°W, however, it increases from 10–15 W m^{-2} to more than 30 W m^{-2} (Figure 7). The gridded distribution explains 67% of the variance; the cosine function explaines an additional 7%. The mean monthly equivalent growth rate of thin ice classes is distributed in a manner similar to energy transfer into the atmosphere. The monthly ice production of more than 30 cm along the Antarctic peninsula is ~3 times higher than that of the remaining Weddell Sea (Figure 8). Here

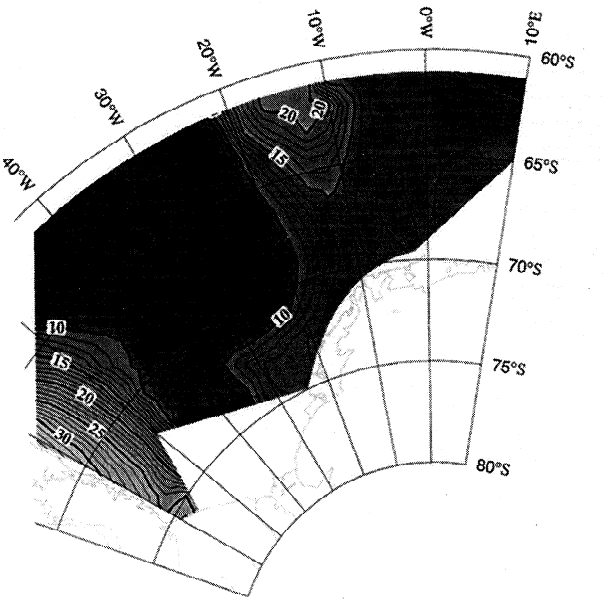

Figure 7. Heat transfer into the atmosphere through all classes of thin ice and open water in W m^{-2} $(month)^{-1}$, weighted by the relative area fraction.

77% of the variance is explained by the gridded field, and 15% is explained by seasonal variation. The salt mass released during ice production shows a comparable behavior. Salt released in leads reaches a maximum of 1.2 kg m^{-2} $(month)^{-1}$ along the Antarctic peninsula (Figure 9). In the central and eastern Weddell Sea the monthly salt release in winter amounts to some 0.4–0.6 kg m^{-2}. With a variance of 80% being due to the gridded field and only 9% being due to the cosine function, the distribution is determined mainly by regional

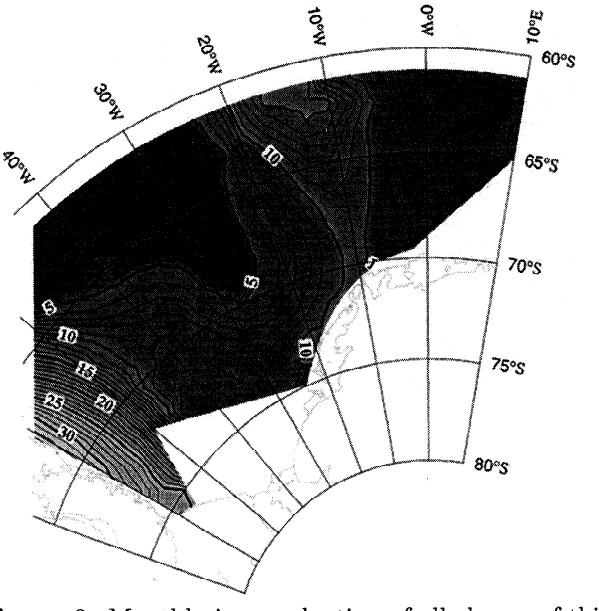

Figure 8. Monthly ice production of all classes of thin ice and open water expressed in equivalent ice growth rates of the total area in centimeters.

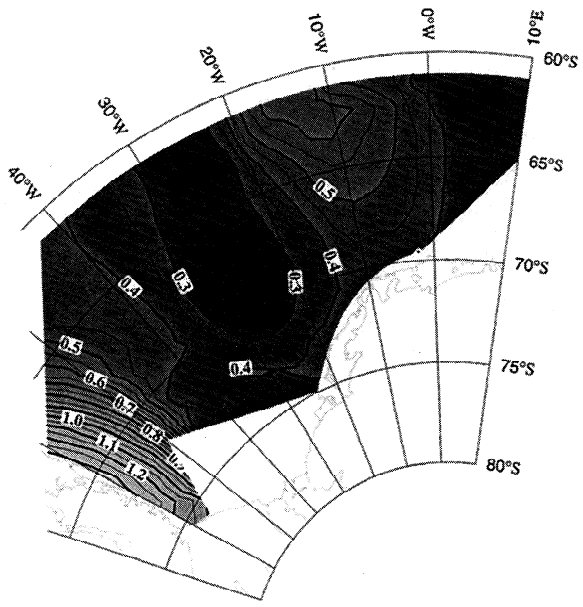

Figure 9. Salt mass released during ice production in leads in kg m^{-2} $(month)^{-1}$.

differences and is fairly independent of seasonal differences in winter.

5. Tidal and Inertial Motion

Ice motion in the Weddell Sea exhibits peaks in the spectra that coincide with diurnal, semidiurnal, and inertial motions [*Rowe et al.*, 1989; *Kottmeier et al.*, 1992; *Padman and Kottmeier*, 2000; *Geiger et al.*, 1998a]. Over the broad continental shelf region in the western Weddell Sea, ice divergence as represented by the buoy array is significantly affected by tidal and inertial currents [*Geiger et al.*, 1998b]. Tides enhance atmospheric heat loss, ice production rates, and brine rejection in winter. The high frequency of the tidal band divergence periods as compared to the weather band divergence periods results in a lower mean ice thickness in leads [*Padman and Kottmeier*, 2000]. In the Weddell Sea, the period of semidiurnal tidal motion almost coincides with that of inertial motion, which varies between 12.3 hours at 76°S and 13.2 hours at 65°S. While tidal motion at ISW is only slightly influenced by inertial motion [*Levine et al.*, 1997], much of the discrepancy between modeled and observed tidal motions over the shelves of the southern and western Weddell Sea can be ascribed to inertial motion [*Padman and Kottmeier*, 2000].

5.1. Local Effects of Tidal and Inertial Motion

On the basis of the above results obtained for a single buoy in the western Weddell Sea the contribution of tidal and inertial motion to the net heat flux, the ice production, and the salt release shall now be evaluated using two model runs with altered input data. In the model runs the buoy field divergence is low-pass filtered at a cutoff frequency of 18 and 30 hours whereas the atmospheric data remain unchanged. Comparison with the unfiltered standard run provides information on processes brought about by motion in the tidal bands. The fraction of thin ice (classes 0–9) is reduced from 34.5% by 0.9% for the 18 hour run and by 2.0% for the 30 hour run. The net heat flux decreases from 40.4 to 39.6 and 38.4 W m^{-2}, respectively. The ice production rate between March 1 and September 5 reaches a maximum for the unfiltered standard run with an equivalent monthly growth rate of 36.2 cm (Figure 10). In the 18 and 30 hour filtered runs, ice production is lower by 5.2 and 12.4%, respectively, than in the standard run. The salt release decreases by 9.9% from 1.42 to 1.28 kg m^{-2} for the 18 hour run and by 22.5% to 1.10 kg m^{-2} for the 30 hour run. Filtering of the divergence thus affects the salt release much more than the ice production rates.

5.2. Regional Effects

To determine the role of tides for salt release in the whole Weddell Sea, a model run as described above was performed for all buoys. The divergences of the buoy fields were low-pass filtered over a period of 36 hours. Spatial distribution of the relative difference of salt release between the standard and the model run reveals a reduction of 5–10% because of filtering in the model run as compared to the standard run for most of the Wed-

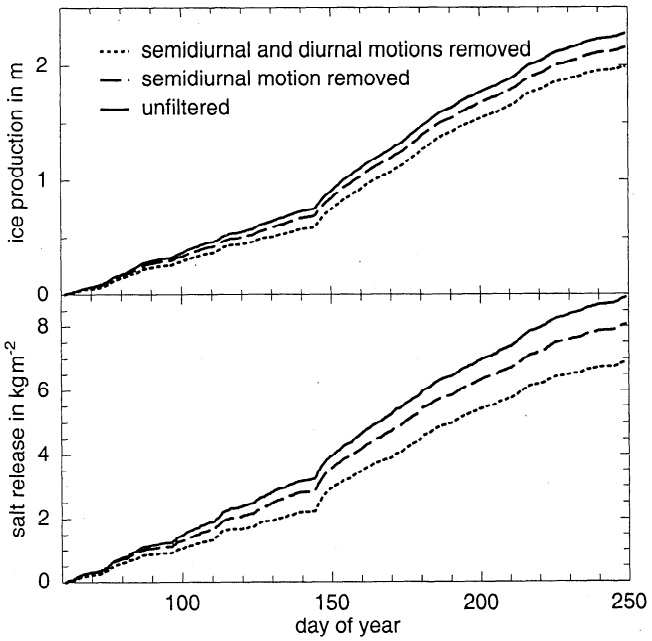

Figure 10. Cumulative development of ice production and salt release for the unfiltered standard run and for low-pass filtered divergence with a cutoff period of 18 and 30 hours. For the period between March 1 and September 5, 2.27 m of ice are produced in the standard run, 2.15 m and 1.99 m in the 18 and 30 hour filtered runs, respectively.

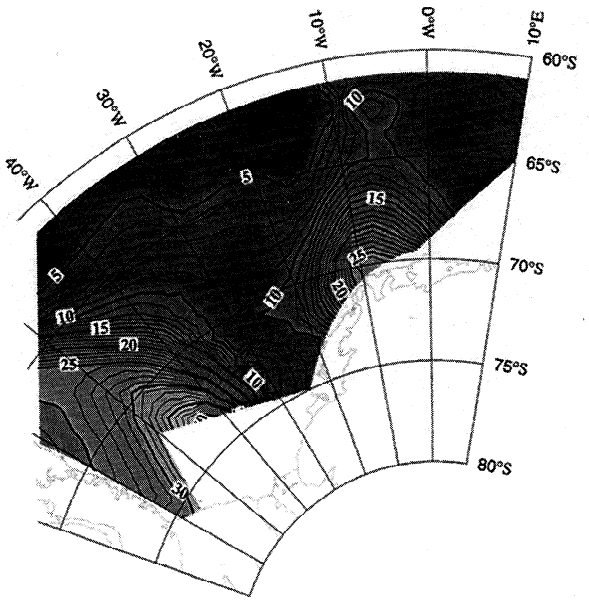

Figure 11. Relative contribution by currents with periods below 36 hours to the total salt release during ice production in percent.

dell Sea (Figure 11). A decrease by 25–30% is observed in the western Weddell Sea. Near Kapp Norvegia along the coast the decrease is some 20–25%.

6. Discussion

Leads in the western Weddell Sea were found to be of striking importance to energy transfer from the ocean to the atmosphere and related processes. If the area fraction covered by leads is taken into account, the net heat flux increases by a factor of 3 to 4 from 12 [*Lytle and Ackley,* 1996] to 40 W m^{-2}. Comparison of the growth rates in section 3 shows that the model overestimates the growth rates by up to 30% for ice thicker than 40 cm, probably because it neglects the snow cover and a time-averaged oceanic heat flux is used. The uncertainty of oceanic heat flux has a greater influence on the contribution of thin ice to total ice production than the overestimated growth rate. Reducing the growth rates by 30% and neglecting the oceanic heat flux cause the contribution of thick ice to total ice production to rise from 8 to 21%.

Tidal and inertial motions affect the energy, mass, and salt balances through ice of a few centimeters in thickness only. Although the influence on the net heat flux into the atmosphere is not pronounced, it should not be neglected when considering regional differences. Motions in the diurnal and semidiurnal bands are of comparable influence. Spectral separation between inertial and semidiurnal tidal motions is impossible. The variability of divergence below a period of 30 hours contributes some 12% to ice production. The most pronounced consequence, however, is the released salt mass reaching a contribution of almost 25%. In this respect, tides play a major role because they change the thickness distribution primarily in the thickness interval of 0–10 cm.

The ice concentrations calculated by the model are highest in the central and western Weddell Sea and decrease slightly toward the Antarctic peninsula. The smaller fraction of thin ice in the central Weddell Sea reduces the contribution of the high heat fluxes in leads to the total net heat transfer to levels found in the eastern Weddell Sea. The maximum heat transfer into the atmosphere along the Antarctic peninsula is mainly due to atmospheric differences and partly to the influence of tidal and inertial motions. Air temperatures in the southwestern Weddell Sea are lower, thus giving rise to higher energy fluxes than in the remaining Weddell Sea. The lack of data on the net heat transfer over thick ice in the Weddell Sea only allows the relative contribution of leads to be estimated. On the basis of the average values given by *McPhee et al.* [1999] and *Lytle and Ackley* [1996] the contributions of leads to the net energy transfer into the atmosphere are found to be ~30% in the eastern and central Weddell Sea, increasing to 70% in the western Weddell Sea.

During ISW and ANZFLUX the conductive heat flux through thick ice and the oceanic heat flux differed by <5 W m^{-2} on average [*Lytle and Ackley,* 1996; *McPhee et al.,* 1999]. With an average maximum area of 90% for thick ice (>90 cm) calculated by the model the difference of both fluxes can be used to evaluate an equivalent monthly ice growth rate under thick ice of 3.8 cm as an upper limit. In the eastern and central Weddell Sea, open water and thin ice account for about twice the amount of ice produced by thick ice. Along the continental shelf in the west, ice growth under thick ice plays a minor role only. About 80% of the total ice mass is formed in leads.

The spatial pattern of salt released in open and refrozen leads (Figure 9) also reflects the distribution of the total salt release far from the coast. Brine production is dominated by ice of <25 cm in thickness. Coastal polynyas, which are not included in our estimates, provide another significant contribution to salt rejection [*Markus et al.,* 1998]. The strong effect on the total brine rejection by divergence variations with a period below 36 hours near Kap Norvegia (Figure 11) can be explained by tides and the spatial variability of the coastal current. Although the low period band contribution to the heat flux, growth rates, and hence salt release is higher than in neighboring regions, the absolute levels are only slightly higher owing to atmospheric forcing. The importance of bathymetry to salt release is significant as is shown by the maximum values over the broad continental shelf. Tidal and inertial variabilities may make up 30% of the total salt mass flux. To compare the contribution by the thin ice classes with those by coastal polynyas, the total salt input is calculated from the data given by *Markus et al.* [1998].

At a mean shelf depth of 400 m a residence time of

a water parcel in the coastal current of 9 years, and an overall salinity increase of 0.39 psu [*Markus et al.*, 1998], the mean monthly salt flux into the ocean due to ice production equals 2.4 kg m^{-2} if freezing is assumed to occur only between March and October. Average salt release in open and refrozen leads along the Antarctic peninsula within 50 km off the coast, i.e., the horizontal extension of coastal polynyas [*Markus et al.*, 1998], is approximately 1.2 kg m^{-2} $(month)^{-1}$. In this region, leads account for 50% of the salinity increase of a water parcel. About 15% of the total increase is due to a variability of ice motion in the tidal and inertial bands. In the southern Weddell Sea, along the margin of the Filchner-Ronne shelf, increased ice production and salt release may be expected because of stronger tidal currents [*Padman and Kottmeier*, 2000]. A detailed analysis based on buoy data in this region is not yet possible as the database is still insufficient.

To estimate the overall effect of leads on the sea ice system, large-scale ice formation in the fall also has to be considered for comparison. In the Weddell Sea an ice cover of ~1 m average thickness forms during fall and winter. The salinity of sea ice with an ice thickness of 1 m typically is 6 psu. Starting from a salinity of 35 psu for seawater in a region that is free of ice in summer, e. g. the central and eastern Weddell Sea sector, the formation of an ice cover of 1 m thickness thus results in a release of approximately 29 kg m^{-2} of salt. In the central and eastern Weddell Sea, leads contribute some 8 cm $(month)^{-1}$ to ice production and an average of 0.5 kg m^{-2} $(month)^{-1}$ to salt release. As the ice cover in these regions typically lasts from March to October, this corresponds to a total ice production of up to 64 cm and a salt release of 4.0 kg m^{-2}. Leads thus contribute ~40% to ice production and 13% to the total rejected salt mass as compared to the effect of initial ice formation.

Over the continental shelf in the western Weddell Sea, however, the situation is different because of the compactness of the sea ice cover. This region is characterized by strongly deformed first and multiyear ice with a mean ice thickness of 1.70 m [*Eicken et al.*, 1994]. Satellite-derived ice concentrations are, in general, above 80% in the summer between 45°W and the Antarctic peninsula and between 80 and 100% in winter depending on the distance from the coast. Using the 20% of open water at the end of summer to form a sea ice cover with a thickness of 1 m, ~5.8 kg m^{-2} of salt are released because of the initial sea ice formation. Spatially averaged, the leads produce some 15 cm of ice and release some 1.2 kg m^{-2} of salt per month. Integrating this effect over the 8 months' winter season, they account for 120 cm of ice and 8.0 kg m^{-2} of salt. This corresponds to 40% of the total ice production and 60% of the total salt release.

7. Conclusion

In this study the energy and mass balances of leads have been analyzed for the first time for a large area of the Weddell Sea. The results emphasize the importance of leads to total energy transfer from the ocean to the atmosphere, to ice production, and to the related salt release by a region covered with sea ice.

Open and refrozen leads contribute between 30 and 70% to the total net heat flux into the atmosphere in an area partially covered by sea ice. The net heat transfer through leads exhibits a general increase from east to west in the Weddell Sea, with a maximum being reached along the Antarctic peninsula. Compared to the central Weddell Sea, this behavior is mainly caused by higher-energy fluxes due to the colder and windier atmosphere. However, the larger percentage of refrozen leads with a young ice cover also contribute to higher heat fluxes since motions in the diurnal and semidiurnal band over the continental shelves cause the ice drift divergence to vary considerably. Although seasonal differences have some influence, the main characteristics are expected to be represented by the spatial distribution. The contribution of leads to the total ice production after the onset of ice cover formation in the fall exceeds 50% in the whole Weddell Sea. Because of the enhanced net heat transfer and the smaller oceanic heat flux in the western Weddell Sea, the total ice production of 30 cm $(month)^{-1}$ in winter is about 3 times larger than that in the central and eastern Weddell Sea. As the salt mass released is directly related to ice production, it exhibits a similar behavior.

Along the continental shelf in the western Weddell Sea, tidal and inertial motions are of major importance to salt release but cause little change in heat transfer. Oceanic currents with periods in the diurnal and semidiurnal bands increase the mean area percentage of thin ice by up to a few centimeters in thickness. The net heat flux increases by 8%, and the ice growth rates increase by 12%. The relatively modest increase in the production of thin ice causes an almost 25% higher salt flux because of the strong decrease of salinity with the rising thickness of thin ice. This may be taken as an additional contribution to the significance of the western shelf region in the formation of bottom water.

The results discussed here imply that neglecting leads in the sea ice cover in mesoscale models may give rise to significant errors. Our model, which is based on buoy data and used to calculate the different quantities characterizing the coupled ocean-ice-atmosphere system for complete area coverage, allows the results to be compared with the output of numerical models. Moreover, investigating agreements with and deviations from space-averaged and time-averaged results obtained by other methods, such as remote sensing, may be pos-

sible. The high time resolution of the buoy data also allows for the performance of a detailed study of isolated events, such as the passing of a low-pressure system and related processes. These data may then be used for further evaluations of the characteristics of the interaction between the ocean, the sea ice, and the atmosphere.

Acknowledgments. The authors gratefully acknowledge the support by E. Andreas, S. F. Ackley, and M. McPhee in providing data on atmospheric properties and heat fluxes. The ECMWF data were contributed by the German Weather Service, Offenbach. SSM/I data were provided by the National Snow and Ice Data Center, University of Colorado, Boulder. Bathymetric information was extracted from "The GEBCO Digital Atlas" of the British Oceanographic Data Centre. Special thanks go to Jörg Hartmann, who developed graphics packages, and whose advice solved many problems. We also thank three anonymous reviewers for their critical comments and advice, which helped to improve the manuscript.

References

Alam, A., and J. A. Curry, Determination of surface turbulent fluxes over leads in Arctic sea ice, *J. Geophys. Res., 102,* 3331-3343, 1997.

Bauer, J., and S. Martin, A model of grease ice growth in small leads, *J. Geophys. Res., 88,* 2917-2925, 1983.

Carmack, E. C., The circulation and mixing in ice-covered waters, in *The Geophysics of Sea Ice,* edited by N. Untersteiner, pp. 641-712, Plenum, New York, 1986.

Cavalieri, D. J., P. Gloersen, and W. J. Campbell, Determination of sea ice parameters with the Nimbus 7 SMMR, *J. Geophys. Res., 89,* 5355-5369, 1984.

Comiso, J., T. C. Grenfell, M. Lange, A. W. Lohanick, R. K. Moore, and P. Wadhams, Microwave remote sensing of the Southern Ocean ice cover, in *Microwave Remote Sensing of Sea Ice, Geophys. Monogr. Ser.,* vol. 68, edited by F. D. Carsey, pp. 243-259, AGU, Washington, D.C., 1992.

Eicken, H., M. A. Lange, H.-W. Hubberten, and P. Wadhams, Characteristics and distribution patterns of snow and meteoric ice in the Weddell Sea and their contribution to the mass balance of sea ice, *Ann. Geophys., 12,* 80-93, 1994.

Fahrbach, E., G. Rohardt, M. Schröder, and V. Strass, Transport and structure of the Weddell Gyre, *Ann. Geophys., 12,* 840-855, 1994a.

Fahrbach, E., R. G. Peterson, G. Rohardt, P. Schlosser, and R. Bayer, Suppression of bottom water formation in the southeastern Weddell Sea, *Deep Sea Res., Part I, 41,* 389-411, 1994b.

Geiger, C. A., S. F. Ackley, and W. D. Hibler III, Sea ice drift and deformation processes in the western Weddell Sea, in *Antartic Sea Ice: Physical Processes, Interactions and Variability, Antarct. Res. Ser.,* vol. 74, edited by M. O. Jeffries, pp. 141-160, AGU, Washington, D.C., 1998a.

Geiger, C. A., W. D. Hibler III, and S. F. Ackley, Modelded versus observed drift and deformation in the western Weddell Sea during 1992, *J. Geophys. Res., 103,* 21,893-21,914, 1998b.

Grenfell, T. C., and G. A. Maykut, The optical properties of ice and snow in the arctic basin, *J. Glaciol., 18,* 445-463, 1977.

Heygster, G., L. Pedersen, J. Turner, C. H. Thomas, T. Hunewinkel, H. Schottmueller, and T. Viehoff, PELICON: Project for estimation of long-term variability of ice concentration, *Technical reports, contract EV5V-CT93-0268(DG 12 DTEE),* Eur. Commun., Brussel, 1996.

Kondo, J., Air-sea bulk transfer coefficients in diabatic conditions, *Boundary Layer Meteorol., 9,* 91-112, 1975.

König-Langlo, G., and E. Augstein, Parameterization of the downward long-wave radiation at the Earth's surface in polar regions, *Meteorol. Z., 3,* 343-347, 1994.

Kottmeier, Ch., and L. Sellmann, Atmospheric and oceanic forcing of Weddell Sea ice motion, *J. Geophys. Res., 101,* 20,809-20,824, 1996.

Kottmeier, Ch., J. Olf, W. Frieden, and R. Roth, Wind forcing and ice motion in the Weddell Sea region, *J. Geophys. Res., 97,* 20,373-20,383, 1992.

Kottmeier, Ch., et al., Wind, temperature and ice motion statistics in the Weddell Sea, *Tech. Doc. WMO/TD No 797,* 48 pp., World Clim. Res. Programme, Geneva, Switzerland, 1997.

Laevastu, T., Factors affecting the temperature of the surface layer of the sea, *Commentat. Phys. Math., 25,* 1-36, 1960.

Ledley, T. S., A coupled energy balance climate-sea ice model: Impact of sea ice on climate, *J. Geophys. Res., 93,* 15,919-15,932, 1988.

Levine, M. D., L. Padman, R. D. Muench, and J. H. Morison, Internal waves and tides in the western Weddell Sea: Observations from Ice Station Weddell, *J. Geophys. Res., 102,* 1073-1089, 1997.

Lytle, V. I., and S. F. Ackley, Heat flux through sea ice in the western Weddell Sea: Convective and conductive transfer processes, *J. Geophys. Res., 101,* 8853-8868, 1996.

Markus, T., Ch. Kottmeier, and E. Fahrbach, Ice formation in coastal polynyas in the Weddell Sea and their impact on oceanic salinity, in *Antartic Sea Ice: Physical Processes, Interactions and Variability, Antarct. Res. Ser.,* vol. 74, edited by M. O. Jeffries, pp. 273-292, AGU, Washington, D.C., 1998.

Martinson, D., Ocean heat and sea ice thickness in the Southern Ocean, in *Ice in the Climate System,* edited by W. Peltier, pp. 597-610, Springer-Verlag, New York, 1994.

Maykut, G. A., Energy exchange over young sea ice in the central Arctic, *J. Geophys. Res., 83,* 3646-3658, 1978.

Maykut, G. A., Large-scale heat exchange and ice production in the central Arctic, *J. Geophys. Res., 87,* 7971-7984, 1982.

Maykut, G. A., The surface heat and mass balance, in *The Geophysics of Sea Ice,* edited by N. Untersteiner, pp. 395-464, Plenum, New York, 1986.

Maykut, G. A., and D. K. Perovich, The role of shortwave radiation in the summer decay of a sea ice cover, *J. Geophys. Res., 92,* 7032-7044, 1987.

McPhee, M. G., S. F. Ackley, P. Guest, B. A. Huber, D. G. Martinson, J. H. Morison, R. D. Muench, L. Padman, and T. P. Stanton, The Antarctic Zone Flux Experiment, *Bull. Am. Meteorol. Soc., 77,* 1221-1232, 1996.

McPhee, M. G., Ch. Kottmeier, and J. H. Morison, Ocean heat flux in the central Weddell Sea during winter, *J. Phys. Ocean., 29,* 1166-1179, 1999.

Melnikov, I., An in situ experimental study of young sea ice formation on an Antarctic lead, *J. Geophys. Res., 100,* 4673-4680, 1995.

Padman, L., and Ch. Kottmeier, High frequency ice motion and divergence in the Weddell Sea, *J. Geophys. Res., 105,* 3379-3400, 2000.

Parkinson, C. L., Length of the sea ice season in the Southern Ocean, 1988-1994, in *Antarctic Sea Ice: Physical Processes, Interactions and Variability, Antarct. Res. Ser.*, vol. 74, edited by M. O. Jeffries, pp. 173-186, AGU, Washington, D.C., 1998.

Parkinson, C. L., and W. M. Washington, A large-scale numerical model of sea ice, *J. Geophys. Res., 84,* 311-337, 1979.

Robertson, R., L. Padman, and M. D. Levine, Fine structure, microstructure, and vertical mixing processes in the upper ocean in the western Weddell Sea, *J. Geophys. Res., 100,* 18,517-18,535, 1995.

Rowe, M. A., C. B. Sear, S. J. Morrison, P. Wadhams, W. S. Limbert, and D. R. Crane, Periodic motions in the Weddell Sea pack ice, *Ann. Glaciol., 12,* 145-151, 1989.

Simmonds, I., and W. F. Budd, Sensitivity of the Southern Hemisphere circulation to leads in the Antarctic pack ice, *Q. J. R. Meteorol. Soc., 117,* 1003-1024, 1991.

Smith, S. D., R. D. Muench, and C. H. Pease, Polynyas and leads: An overview of physical processes and environment, *J. Geophys. Res., 95,* 9461-9475, 1990.

Steffen, K., and A. Schweiger, NASA team algorithm for sea ice concentration retrieval from Defense Meteorological Satellite Program Special Sensor Microwave Imager: Comparison with Landsat satellite imagery, *J. Geophys. Res., 96,* 21,971-21,987, 1991.

Steffen, K., J. Key, D. J. Cavalieri, J. Comiso, P. Gloersen, K. S. Germain, and I. Rubinstein, The estimation of geophysical parameters using passive microwave algorithms, in *Microwave Remote Sensing of Sea Ice, Geophys. Monogr. Ser.,* vol. 68, edited by F. D. Carsey, pp. 201-231, AGU, Washington, D.C., 1992.

Strass, V. H., and E. Fahrbach, Temporal and regional variation of sea ice draft and coverage in the Weddell Sea obtained from upward looking sonars, in *Antarctic Sea Ice: Physical Processes, Interactions and Variability, Antarct. Res. Ser.,* vol. 74, edited by M. O. Jeffries, pp. 123-140, AGU, Washington, D.C., 1998.

Thorndike, A. S., Kinematics of sea ice, in *The Geophysics of Sea Ice,* edited by N. Untersteiner, pp. 489-550, Plenum, New York, 1986.

Veihelmann, B., F. S. Olesen, and Cc. Kottmeier, Sea ice surface temperature in the Weddell Sea (Antarctica) from drifting buoy and AVHRR data, *Cold Reg. Sci. Technol.,* in press, 2000.

Vihma, T., J. Launiainen, and J. Uotila, Weddell Sea ice drift: Kinematics and wind forcing, *J. Geophys. Res., 101,* 18,279-18,296, 1996.

Wakatsuchi, M., Brine exclusion process from growing sea ice, *Contrib. Inst. Low Temp. Sci. A, Hokkaido Univ. Ser., 33,* 29-65, 1983.

Zillmann, J. W., A study of some aspects of the radiation and heat budgets of the Southern Hemisphere oceans, *Meteorol. Stud., 26,* 562 pp., Bur. of Meteorol., Dep. of Interior, Canberra, Canberra, A. C. T., Australia, 1972.

O. Eisen, Alfred-Wegener-Institut für Polar- und Meeresforschung, Postfach 120161, 27515 Bremerhaven, Germany. (oeisen@awi-bremerhaven.de)

C. Kottmeier, Institut für Meteorologie und Klimaforschung, Universität Karlsruhe, Kaiserstr. 12, 76133 Karlsruhe, Germany. (ckottmei@imk.fzk.de)

(Received March 19, 1999; revised December 9, 1999; accepted March 10, 2000.)